A germanium hybrid pixel detector with 55μm pixel size and 65,000 channels

2014 JINST 9 P12003

(http://iopscience.iop.org/1748-0221/9/12/P12003)

PUBLISHED BY IOP PUBLISHING FOR SISSA MEDIALAB

RECEIVED: *October 6, 2014*
ACCEPTED: *November 7, 2014*
PUBLISHED: *December 4, 2014*

A germanium hybrid pixel detector with 55μm pixel size and 65,000 channels

D. Pennicard,[a,1] **B. Struth,**[a] **H. Hirsemann,**[a] **M. Sarajlic,**[a] **S. Smoljanin,**[a] **M. Zuvic,**[b] **M.O. Lampert,**[b] **T. Fritzsch,**[c] **M. Rothermund**[c] **and H. Graafsma**[a]

[a] *DESY,*
Notkestrasse 85, Hamburg 22607, Germany
[b] *Canberra France Speciality Detectors,*
1 chemin de la Roseraie, Parc des Tanneries, 67380 Lingolsheim, France
[c] *Fraunhofer IZM,*
Gustav-Meyer-Allee 25, 13355 Berlin, Germany

E-mail: david.pennicard@desy.de

ABSTRACT: Hybrid pixel semiconductor detectors provide high performance through a combination of direct detection, a relatively small pixel size, fast readout and sophisticated signal processing circuitry in each pixel. For X-ray detection above 20 keV, high-Z sensor layers rather than silicon are needed to achieve high quantum efficiency, but many high-Z materials such as GaAs and CdTe often suffer from poor material properties or nonuniformities. Germanium is available in large wafers of extremely high quality, making it an appealing option for high-performance hybrid pixel X-ray detectors, but suitable technologies for finely pixelating and bump-bonding germanium have not previously been available.

A finely-pixelated germanium photodiode sensor with a 256 by 256 array of 55 μm pixels has been produced. The sensor has an n-on-p structure, with 700 μm thickness. Using a low-temperature indium bump process, this sensor has been bonded to the Medipix3RX photon-counting readout chip. Tests with the LAMBDA readout system have shown that the detector works successfully, with a high bond yield and higher image uniformity than comparable high-Z systems. During cooling, the system is functional around -80°C (with warmer temperatures resulting in excessive leakage current), with -100°C sufficient for good performance.

KEYWORDS: Solid state detectors; X-ray detectors; Materials for solid-state detectors; Hybrid detectors

[1] Corresponding author.

doi:10.1088/1748-0221/9/12/P12003

Contents

2014 JINST 9 P12003

1 Hybrid pixel technology and germanium

In a hybrid pixel detector, a pixelated semiconductor sensor such as a photodiode is bonded face-to-face to a readout chip that provides an electronics channel per pixel. As a result, the detector provides direct detection and makes it possible to combine sophisticated signal processing with a relatively small pixel size. While these detectors were first adopted for particle physics, they play an increasingly important role in X-ray detection, particularly at synchrotrons and free electron lasers (FELs). The most common approach for X-ray detection is photon counting, where for each photon absorbed in the sensor the energy deposited is compared to a user-defined threshold, and a counter in the pixel is incremented for each hit that exceeds the threshold. This approach is used for example in Medipix3 [1] and Pilatus [2], and allows effectively noise free performance and energy discrimination capability. In Medipix3, it is also possible to do spectroscopic imaging by binning photon hits into a series of energy ranges. The hybrid pixel structure allows fast readout, and with other readout chip designs it is possible to have fast integrating detectors with extremely high dynamic range [3], spectroscopic detectors with a high number of channels [4] and detectors that provide a combination of time, position and energy resolution [5].

Although silicon hybrid pixel detectors are suitable for experiments at moderate X-ray energies, at energies above about 20 keV the absorption efficiency of silicon rapidly becomes poor. So, efficient hybrid pixel detectors for hard X-ray detection need to be built using semiconductors with

higher atomic number ("high Z"). Currently, common options for this include cadmium telluride (CdTe) and gallium arsenide (GaAs). As these are compound semiconductors, it is difficult to produce large, defect-free wafers of these materials. While CdTe now is available with relatively good carrier transport properties, pixel detectors based on CdTe often suffer from nonuniformities and polarization effects [6], and likewise it is difficult to produce GaAs with a combination of high resistivity, long carrier lifetime and high uniformity [7].

In contrast, high-purity germanium is already available in large wafers of excellent quality, making it an appealing option for detectors. However, there are a few obstacles to using germanium in a hybrid pixel detector. Firstly, existing germanium detectors are typically based on either large pixels (of order mm size) or fine-pitch strip detectors. So, fine-pitch pixel detector fabrication technologies needed to be developed, as described in section 2. Secondly, germanium sensors are vulnerable to damage during processing. In silicon detectors, silicon oxide and nitride provide relatively tough and stable passivation layers, whereas passivation layers in germanium detectors are more easily damaged. Additionally, high-temperature processing can induce diffusion of impurities into the germanium, harming the detector qualities. So, germanium pixel hybrid pixel detectors need to be bump bonded at low temperature, with a process that does not remove the passivation. The indium bonding process for germanium detectors is described in section 3. Finally, due to germanium's narrow bandgap, it needs to be cooled during operation to reduce its leakage current. In the case of a typical photon counting detector, the pixel volume is small, and extremely high spectroscopic performance is not required, so higher leakage current can be tolerated; as shown in section 5.3, operation below -80°C is sufficient. Nevertheless, the cooling and readout system need to be designed to cope with this.

1.1 The Medipix3 readout chip

In this project, a germanium hybrid pixel detector was built using the Medipix3 photon-counting readout chip [1] and the LAMBDA [8] readout system. The Medipix3 chip was produced by the Medipix3 collaboration, with the chip design being done at CERN. Unless otherwise stated, all the work in this paper was done with the Medipix3RX [9] chip. It has a flexible design, with each basic pixel of 55 μm containing a charge-sensitive preamplifier, a shaping amplifier, two sets of discriminators, a variety of interpixel communication circuits, and two counters. The chip has an array of 256 by 256 pixels, giving a pixel array area of 14.1 mm by 14.1mm. The chip can be configured for a range of applications; for example, the two counters can be used to divide photon hits into two energy bins (with charge-sharing compensation) or to allow fast deadtime-free readout. By bonding the chip to a sensor with 110 μm pitch, the detector can be used in a mode that provides 8 sets of thresholding circuitry and 8 counters, for spectroscopic imaging.

For working with germanium detectors, the chip's amplifier design should be considered. The preamplifier in each pixel has a Krummenacher design, which allows hole or electron readout and has a circuit that compensates for leakage current. The pixel can compensate up to 30 nA of leakage current, with the maximum compensation being controlled by a current source called Ikrum. However, increasing leakage current will increase the noise of each pixel. The shaping amplifier has a shaping time of 120 ns, which means that a leakage current of 1 nA per pixel (i.e. 330 nA/mm^2) would correspond to a shot noise of approximately 37 electrons; since the electronic noise of the chip is 72 electrons, achieving this current level or below is sufficient to avoid a large increase in noise.

2014 JINST 9 P12003

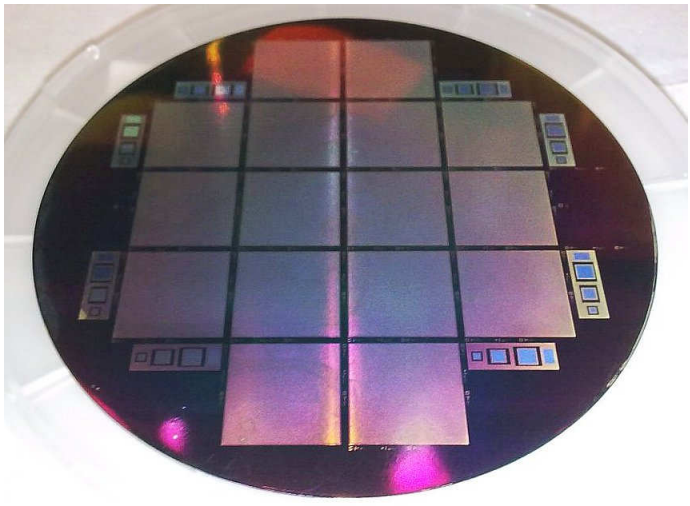

Figure 1. A 90 mm high-purity Germanium wafer with 16 Medipix3-compatible sensors, each with a 256 x 256 array of 55 μm pixels. The wafer is 700 μm-thick p-type material.

2 Production of finely pixelated germanium sensors

After performing tooling tests, a set of Medipix-compatible sensors were produced on two 90 mm wafers of p-type high-purity germanium. The process flow is based on a double-sided wafer process. The sensors have a photodiode structure, with the pixels on the n-type implant side (electron collection). The HV side, or entrance window, is based on a p-type implantation. A completed wafer is shown in figure 1. Each wafer has 16 sensors with 55 μm pixel size and a layout of 256 by 256 pixels (65536 total), matching the Medipix3 chip. Around the pixel array are guard ring structures with a total width of 750 μm. After processing, the sensors have a thickness of 700 μm. This thickness was chosen as a compromise between performance and mechanical stability — for the prototype detectors, using a thinner sensor reduces charge-sharing effects and bulk leakage current, but makes it more difficult to safely handle the wafers during processing.

The wafers included test structures for measuring leakage current and depletion voltages at different temperatures. At a temperature of -100°C the sensor's depletion voltage was 20V. At -70°C the depletion voltage increased to 40V, and at warmer temperatures the depletion voltage increased rapidly. Tests of 1 mm^2 diodes showed a bulk leakage current of 10 nA at -70°C, which is well below the 330 nA/mm^2 required for good performance with the Medipix3 chip. However, the current in the guard ring was around 5 orders of magnitude higher, and increased linearly with bias voltage, so the guard ring current in the chip is liable to be larger than the pixel array current. It should also be noted that the fine pixelation and bump processing may increase the current in the sensors, for example due to surface effects.

3 Low-temperature indium bonding of germanium

3.1 Selection of indium bonding process

Bonding germanium sensors to readout chips presents two sets of challenges. Firstly, germanium sensors can be damaged by high temperatures and some chemical processing steps. In particular,

2014 JINST 9 P12003

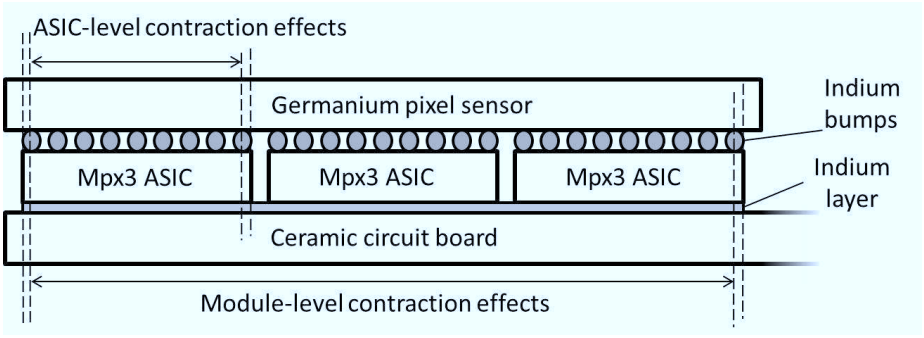

Figure 2. A diagram of a germanium hybrid pixel module, indicating thermal contraction mismatch between the germanium sensor and the silicon readout chip, and also between the sensor and the circuit board.

thermal processing tests on germanium diodes showed an increase in leakage current after heating to temperatures above 100°C. Typical bump bonding techniques involve bonding the two chips with solder, which needs to be heated above its melting point to make a strong bond, making many methods unsuitable. Secondly, the germanium sensor has a coefficient of thermal expansion (CTE) of 6 ppm/K, compared to 2.5 ppm/K for silicon, which means that there is a mismatch in contraction during cooling, which may damage the bonds. Figure 2 shows a diagram of a germanium hybrid pixel module, indicating sources of thermal contraction mismatch. It can be seen that this effect will increase not only with the CTE mismatch and the change in temperature between room temperature and operation, but also the chip size.

Indium bump bonding techniques have been shown to avoid both of these problems [10]. Indium is a soft and ductile metal. By depositing In bumps on both the readout chip and the sensor, they can be bonded together at temperatures below 100°C using a thermocompression process, where the parts are pressed together with high pressure and moderate temperature (70°C) while applying sonic energy to ensure that any oxide layer on the surface of the bumps is broken. Furthermore, since In is ductile even at low temperatures, when the detector assembly is cooled the bump bonds can flow slightly to accommodate the mismatch in thermal contraction between the sensor and readout chip. In reference [11], this approach was shown to work with a hybrid pixel detector with a GaAs quantum well structure. This sensor had a slightly higher CTE than germanium of 7 ppm/K (i.e. a larger mismatch with silicon), an area of 20.5 mm by 20.5 mm, a pixel size of 20 μm and an operating temperature of 60K. Many of these requirements are considerably more demanding than the germanium pixel design, particularly the much smaller pixel size and deeper cooling, so the bump bonded germanium sensor should work fine at low temperature. If the germanium detector is operated at -100°C then the mismatch in thermal contraction between the germanium and silicon will amount to 4.5 μm at the corners of the chip, which is small compared to the bump size.

Large hybrid pixel detector modules can be produced by bonding multiple readout chips to a single large sensor. In a large module, the mismatch between the pixels on the sensor and a given readout chip will be the same as for a single chip, but as shown in figure 2 there will be an additional mismatch: the mismatch between the germanium sensor and the circuit board the detector assembly sits on. This can be avoided by choosing a circuit board material that matches the CTE of germanium, as discussed in section 4.1.

2014 JINST 9 P12003

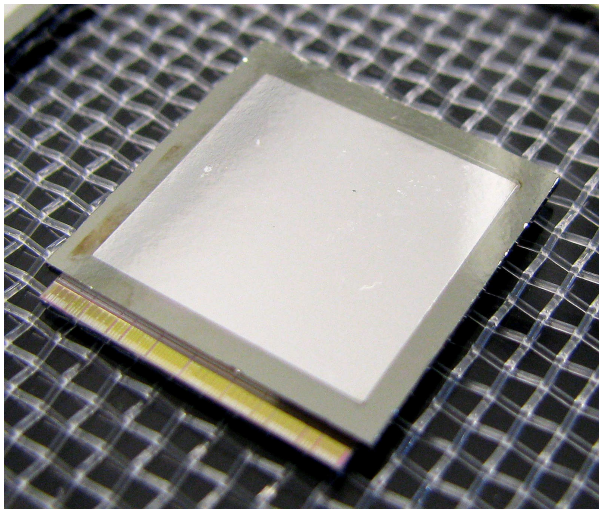

Figure 3. A single germanium sensor Indium bump bonded to a Medipix3 readout chip.

3.2 Indium bump bonding at Fraunhofer IZM

The germanium sensors were Indium bump bonded to Medipix3RX chips at Fraunhofer IZM (Berlin). The bumps were deposited on both the sensors and readout chips by an electroplating process, which can produce pillar-shaped bumps with a fine pitch without using a reflow step. This was done using a modified version of their existing bump process, which is described in detail in ref. [12]. To optimize the process, a series of tests were first made with Germanium diode test structures. These were subjected to a range of processing conditions in order to find a set of parameters that would not damage the surface of the sensors or degrade their current-voltage characteristics. Similarly, the flip-chip assembly conditions were optimized using test structures made from non-detector-grade Germanium.

The bump deposition process starts with a resputtering step to remove the oxide from the pixel metallization pads followed by a sputter deposition of a TiW/Cu plating base layer. This layer stack acts as a adhesion layer and as a seedlayer for the electroplating process. A layer of photoresist was deposited and patterned to define bump openings with a diameter of 34 µm. Then the indium bumps were grown, starting with the deposition of a Under-Bump Metallisation (UBM) socket and followed by an indium height of up to 10 µm. After removing the photoresist, the Cu and TiW plating base layer were removed by wet chemical etching.

After electroplating the bumps on both sensor and readout chip wafers, the wafers were diced. A flip-chip thermocompression bond process was chosen for the assembly. During the bond process force and temperature were applied, which create the micro joint. Due to the deposition of In on both sides it is possible to bond the readout chip to the sensor in a thermocompression bonding step with a temperature below the melting point of In. The readout chip was bonded at a temperature of 70°C. A finished Germanium sensor bonded to a Medipix3 chip is shown in figure 3.

4 The LAMBDA readout system and test measurement setup

DESY have developed a readout system for the Medipix3 chip, called LAMBDA (Large Area Medipix3 Based Detector Array) [8]. A single LAMBDA module detector head has space for up

2014 JINST 9 P12003

to 12 Medipix3 chips mounted on a circuit board in a 6 by 2 layout. The board can be used to operate a single large sensor of 85 mm by 28 mm bonded to 12 chips (with 1536 by 512 pixels of 55 µm size), two smaller sensors of 42 mm by 28 mm each bonded to 6 chips, or smaller prototype sensors. The detector head is mounted on a copper frame for cooling, and connected to high-speed readout electronics to form a single module. Multiple modules can be tiled together to cover a larger area.

4.1 Detector head design and assembly

For use with a germanium sensor, the detector head had to be designed to cope with low-temperature operation. The detector head uses a circuit board made of low-temperature co-fired ceramic (LTCC). This material was chosen because it has a coefficient of thermal expansion of around 6 ppm/K, matching germanium. So, this means that if large germanium detectors bonded to multiple readout chips are mounted on it, there will not be large mismatches in thermal contraction when the system is cooled. The ceramic board has higher thermal conductivity than standard FR4 and contains silver-filled vias to increase thermal conductivity between the sensor assembly on the front of the ceramic and the cooling block on the back. For a power per chip of 1.5W, the estimated temperature difference across the thickness of the ceramic is 6°C.

When building a system operating at room temperature, the detector assembly is mounted on the LTCC board with thermally and electrically conductive glue, and in turn the LTCC board is glued to the mechanics. However, it was found that glue layers performed poorly when cooled to low temperature, even when using glues intended for lower-temperature operation — in particular, the cooling frame tended to come unglued from the ceramic board. Instead, a layer of indium foil was placed between the sensor assembly and the ceramic, and the sensor was pressed down using a 1 mm-thick piece of plastic (Vespel). The Vespel was bent so that it would act as a spring. In future, this could be replaced by a frame around the sensor's guard ring area, so that the pixel array can be left uncovered. Likewise, the ceramic board was clamped onto the cooling mechanics with a layer of indium between them. The assembled detector head with a single Ge assembly is shown in figure 4.

4.2 Readout system

Previously, two versions of the LAMBDA readout electronics were developed: a early prototype system using USB readout [13], and a high-speed readout system using 10 Gigabit Ethernet and a more sophisticated readout board [8]. Although the high-speed readout system has been used with other sensor materials, the prototype readout system was used to test the germanium sensor due to its smaller size and lower power consumption. The prototype readout consists of a voltage regulator board providing power to the detector head, and a readout board with an FPGA for detector control and a USB2 link for communication with the control PC.

4.3 Vacuum chamber and cooling mechanics

The detector head and prototype readout system were tested in a vacuum test chamber, as shown in figure 5. The detector's cooling mechanics were bolted to a larger cooling block attached to a Cryotiger (a compressor-based cooling system). A miniature X-ray tube with a Ag anode, 50kV

2014 JINST 9 P12003

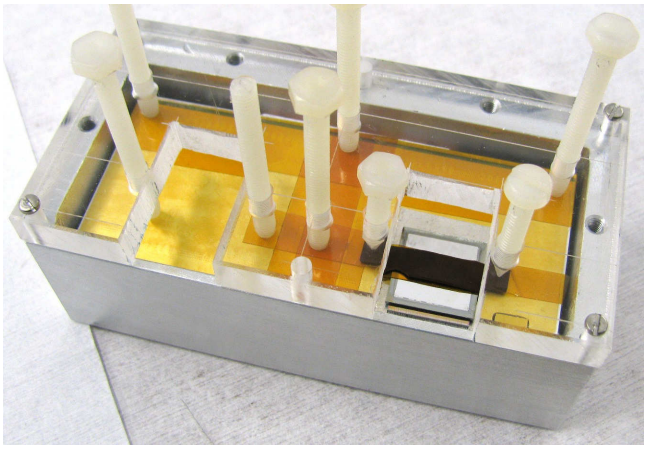

Figure 4. A single chip germanium detector mounted on a ceramic circuit board, which is then mounted on a cooling block inside an aluminium frame. Two plastic screws hold a piece of Vespel on top of the detector, which presses the detector onto the board like a spring. A layer of indium foil then gives a good thermal contact between the detector and the board.

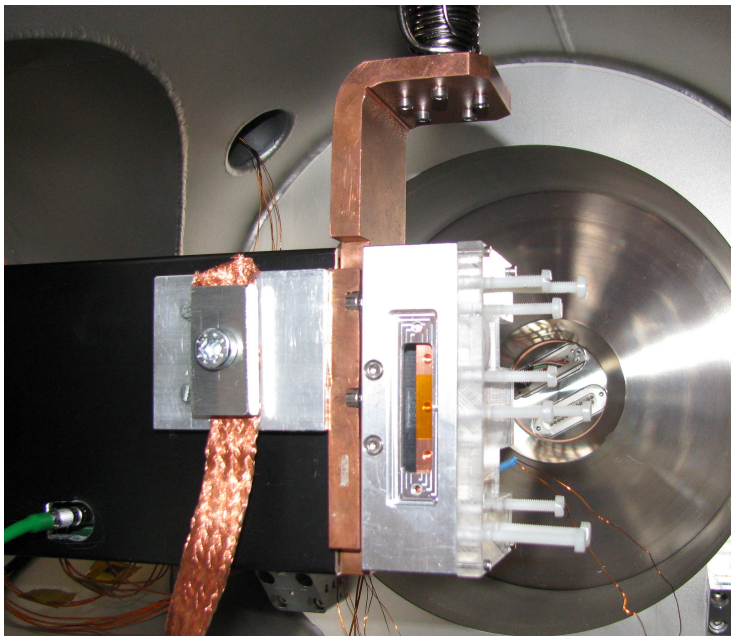

Figure 5. The single chip Germanium system inside a vacuum test chamber. The detector head is connected to a Cryotiger cooler from above . The readout electronics (inside a housing) are connected to power and signal output cables via a connector on the chamber wall. A miniature X-ray tube is mounted in the wall of the chamber (not visible).

maximum voltage and 1 mm Al filter was mounted in the wall of the chamber to allow X-ray testing. Temperature sensors were connected both to the detector's cooling mechanics, and the surface of the ceramic circuit board.

After allowing the system to outgas at room temperature, the system could be cooled under vacuum to a minimum of -130°C. Under these conditions, the pressure in the chamber was 1×10^{-6}

2014 JINST 9 P12003

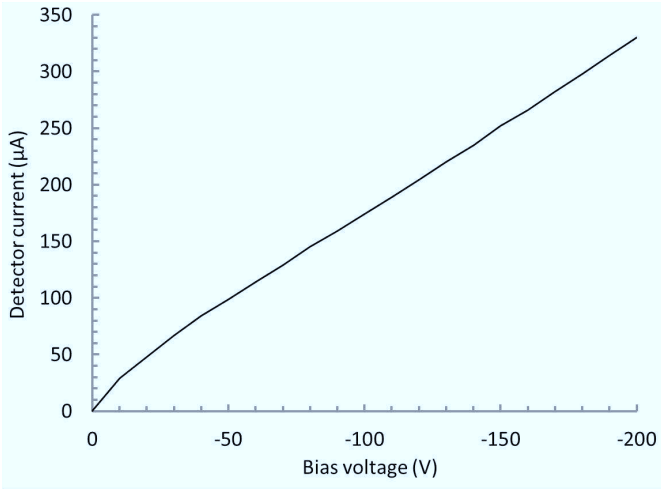

Figure 6. Total leakage current with absolute value of bias voltage in the germanium sensor at -120°C.

mbar. When the detector was powered up, the sensor assembly warmed up by around 20°C due to heating by the readout chip, which had a power consumption of 1.3W. (The details of measuring the sensor temperature are explained in the next section.)

5 Test results

5.1 Current-voltage characteristics

A series of current-voltage measurements were made with the Medipix3 chips unpowered. Under these conditions, the sensor assembly produced negligible heating power, so the temperature sensors on the cooling mechanics and ceramic board would give an accurate measurement of the sensor temperature. Firstly, current-voltage measurments were made with the sensor at -120°C. This was done by monitoring the current in the power supply, so the total of bulk current in the pixels and edge current in the guard ring was measured. The results are shown in figure 6. The results show a relatively high current of 174 μA at -100V, and a linear increase in current with bias. The previous results from test diodes showed that the total current here is likely to be almost entirely guard ring current.

The leakage current was measured with varying temperature on the sensor, keeping a bias of -100V. The results are shown in figure 7. The rate of carrier generation in a semiconductor is expected to be proportional to $T^{3/2}e^{-E_a/2kT}$, and over limited temperature ranges the exponential factor will dominate. So, the plot shows temperature on a logarithmic scale, and the spacing on the temperature scale is proportional to $-1/T$. The graph follows a straight line, which shows that the variation in current with temperature behaves as expected. Interestingly, the corresponding activation energy E_a is 0.21 eV, which is much less than the bandgap of germanium, which is 0.67 eV. This suggests that the dark current is dominated by Shockley-Read-Hall generation, where electron-hole pairs are generated by a series of excitations via defect levels in the bandgap, rather than direct excitation of electrons from the valence to the conduction band [14]. This is reasonable, given that the cut edges of the germanium sensor will have a high density of defects.

2014 JINST 9 P12003

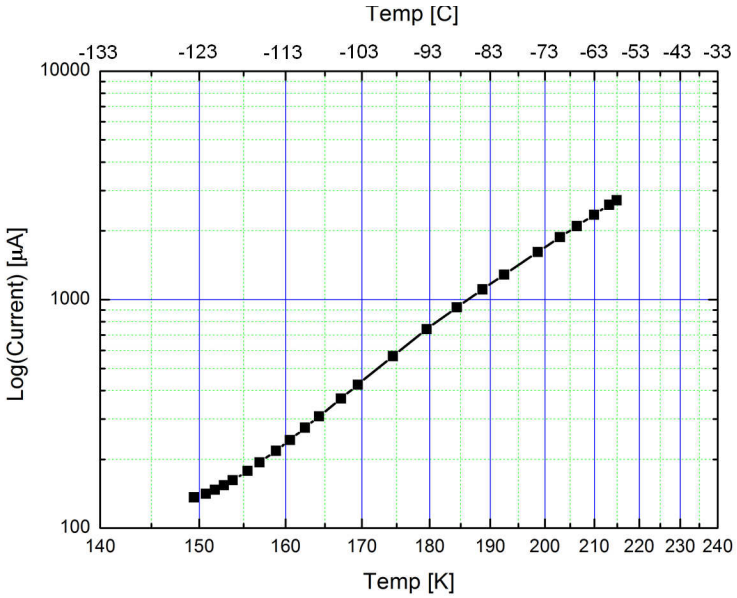

Figure 7. Total leakage current with sensor temperature in the germanium sensor with -100V bias.

In measurements with the detector fully powered, the leakage current in the sensor was monitored, and the current-voltage results shown in figure 7 were used to obtain a measurement of the sensor temperature. This was necessary because the heat generated by the readout chips during operation resulted in temperature differences between the temperature sensors, which were mounted on the cooling mechanics and circuit board, and the sensor itself.

5.2 Calibration and X-ray detection

In a hybrid pixel detector, there are inevitably pixel-to-pixel variations in the readout channels. In Medipix3, the main result of this variation is a pixel-to-pixel variation in the effective threshold for photon counting. To reduce this variation, each pixel contains a 5-bit DAC which can be used to fine-tune its threshold setting. Before testing with X-rays, an equalisation was performed to find the best adjustment for each pixel, based on the position of the noise edge. Previous tests with a bare Medipix3RX chip had showed an RMS spread in the noise edge of 1.6 threshold steps at room temperature after equalisation, and a spread of 2.0 threshold steps at -70°C. So, this showed that the pixel-to-pixel variation worsens at lower temperatures. The germanium sensor at -100°C showed a pixel-to-pixel variation in the noise edge of 2.3 threshold steps, which was in line with the bare chip results as expected, and corresponds to 115 electrons for present chip settings.

The germanium sensor was tested with uniform illumination from the miniature Ag X-ray tube at 50kV. using a threshold setting of 65 (7.5 keV), a bias of -100V and -100°C temperature. The resulting flat image is shown in figure 8. 96.7% of pixels are functional, with a total of 2150 bad pixels (i.e. those with less than 0.5 or more than 1.5 times the mean number of counts). It can be seen that the response is generally uniform across the detector. A faint shadow can be seen horizontally across the central region of the chip, due to the Vespel that placed over the detector to hold it in place. Most of the nonworking pixels are insensitive pixels around the edges of the detector, and if the edge regions are excluded the yield of working pixels becomes 99.77%. As

2014 JINST 9 P12003

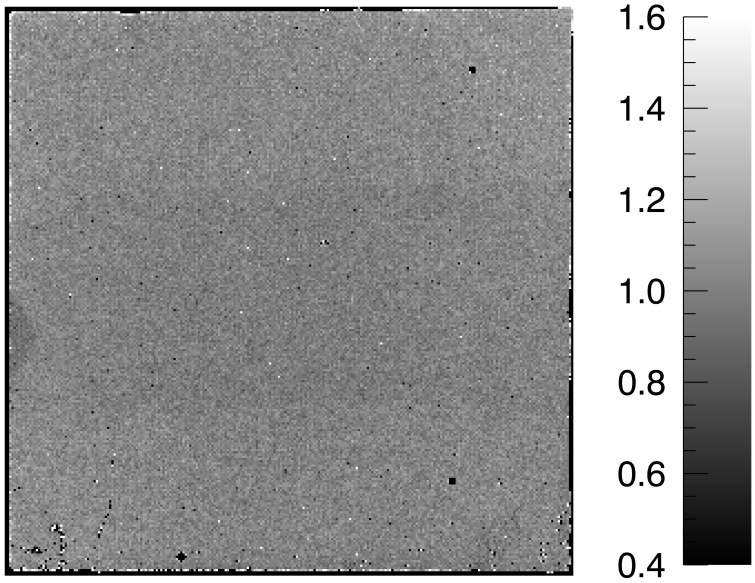

Figure 8. Flat field image taken with the germanium detector under uniform illumination from an Ag X-ray tube at 50kV, with -100V bias voltage, -100°C temperature and a threshold of 7.5 keV. The image is the sum of 20 acquisitions, each lasting 1s.

shown in section 5.3 the width of this insensitive region increases at warmer temperatures. This indicates that the pixels are nonfunctional due to excessive leakage current, rather than the pixels being disconnected; if a pixel has excessively high current, then its preamplifier becomes saturated and a photon hit will no longer produce a signal pulse. Overall, these results show the germanium sensor is functioning well, aside from the high current around the edges of the detector.

Figure 9 shows a histogram of the number of counts seen in each pixel of the detector. The histogram is normalised by the average value. The RMS spread in the measured intensity is 8.8% for the whole image, or 7.8% if we consider only the central or upper region to eliminate the effect of the slight "shadowed" region created by the Vespel piece (which has 5% lower intensity). This variation will at least in part be due to pixel-to-pixel variations in the readout electronics. As described previously, the detector has a threshold dispersion of about 115 electrons RMS after equalisation using the noise edge. Furthermore, the Medipix3RX chip at room temperature has a pixel-to-pixel gain variation of around 4% RMS, corresponding to 100 electrons or 300 eV variation at a threshold setting of 7.5 keV. Assuming these can be added in quadrature, with a threshold of 7.5 keV one would expect an overall pixel-to-pixel variation in effective threshold level of 180 electrons or 540 eV. The results presented in figure 12 show how the count rate on the detector varies with threshold level — this is discussed in more detail later in this section. Using these results, the expected pixel-to-pixel threshold variation would produce a variation in flat-field intensity of 5.5% RMS. So, the pixel-to-pixel variation is greater than can be explained purely by the expected variation in the readout chip. This either implies that the sensor itself makes a significant contribution to the flat-field nonuniformity (of order 6%) or that the low operating temperature and relatively high sensor current result in a greater than expected variation in gain from one readout channel to another.

2014 JINST 9 P12003

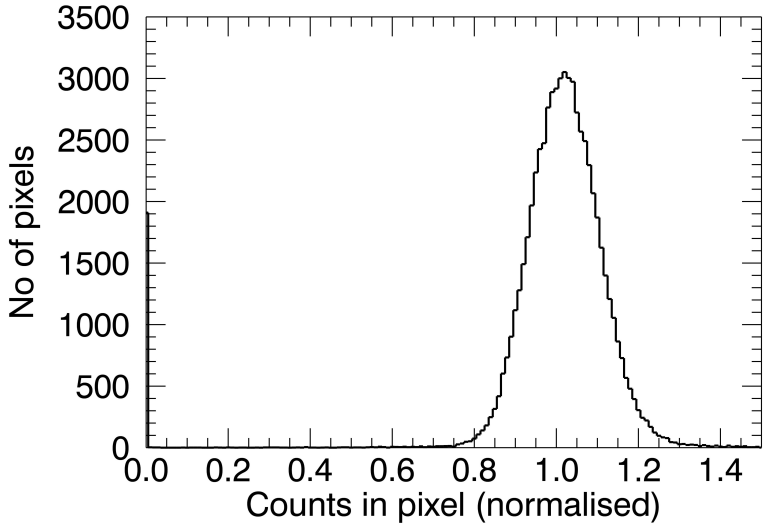

Figure 9. Histogram showing distribution of counts in the image from figure 8. The number of counts is normalised by the average value.

As an illustration of imaging with the detector, figure 10 shows an X-ray image of a USB stick placed in the vacuum chamber (without flat-field correction). A threshold of 7.5 keV and a bias of -200V were used. Figure 11 shows an example of the effect of flat-field correction. The upper-left image (A) shows another image of the USB stick. This image was taken with -100V bias, and shows greater pixel-to-pixel variation in response than figure 10. This is due to the increased charge sharing at lower bias voltage; for a given level of pixel-to-pixel variation in threshold, the pixel-to-pixel variation in the number of counts will depend on the proportion of "hits" are close to the threshold level, and this will increase with charge sharing. (As an illustration, if there was no charge sharing, then as long as the threshold level was sufficiently far from the zero level and the photon energy to prevent noise fluctuations having an effect, each hit would be counted exactly once regardless of the particular threshold value.) The upper-right image (B) then shows the same image with flat-field correction applied, and the pixel-to-pixel uniformity is substantially improved. The lower images show a zoom-in into each picture to make the comparison clearer.

Figure 12 shows the results of a threshold scan performed with the detector, where the threshold setting was varied step-by-step, an image taken for 1s at each step, and the total number of counts in each image found. (The figure shows the total counts at each threshold step, rather than a differential spectrum.) The shape of the curve will correspond to a convolution of the X-ray tube integral spectrum with the response of the detector. For a monochromatic source with low charge sharing, one would expect an S-shaped curve, with the position of the "S" corresponding to the monochromatic photon energy, thus making it possible to gain accurate energy calibration of the detector. In this case, the combination of a broad tube spectrum and higher charge sharing due to the sensor thickness mean that clear information cannot be extracted from the curve. However, using the HORUS simulation code [15] to simulate the detector response to the estimated tube spectrum, it was found that the experimental results agree with the expected results from simulation, as shown in the figure. The comparison between simulated and experimental results was

2014 JINST 9 P12003

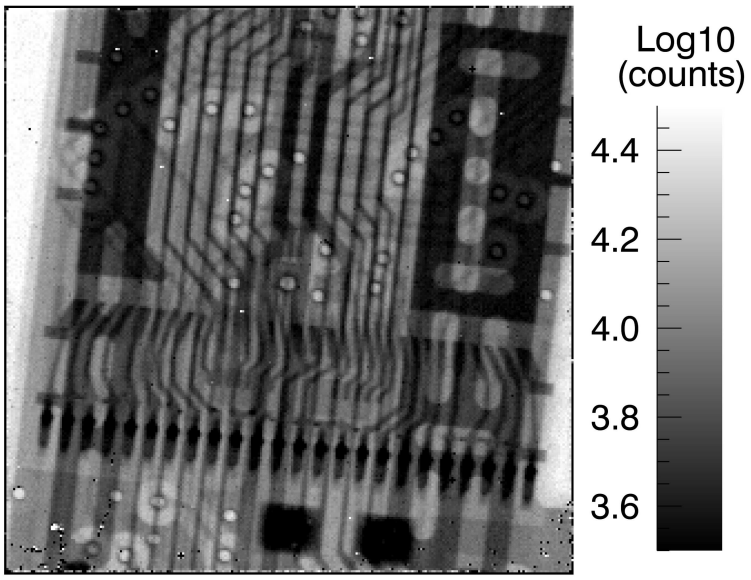

Figure 10. Image of part of a USB stick, taken with the detector at -200V bias, -100°C temperature and a threshold of 7.5 keV. A logarithmic scale is used. The image is the sum of 300 acquisitions, each of 1s.

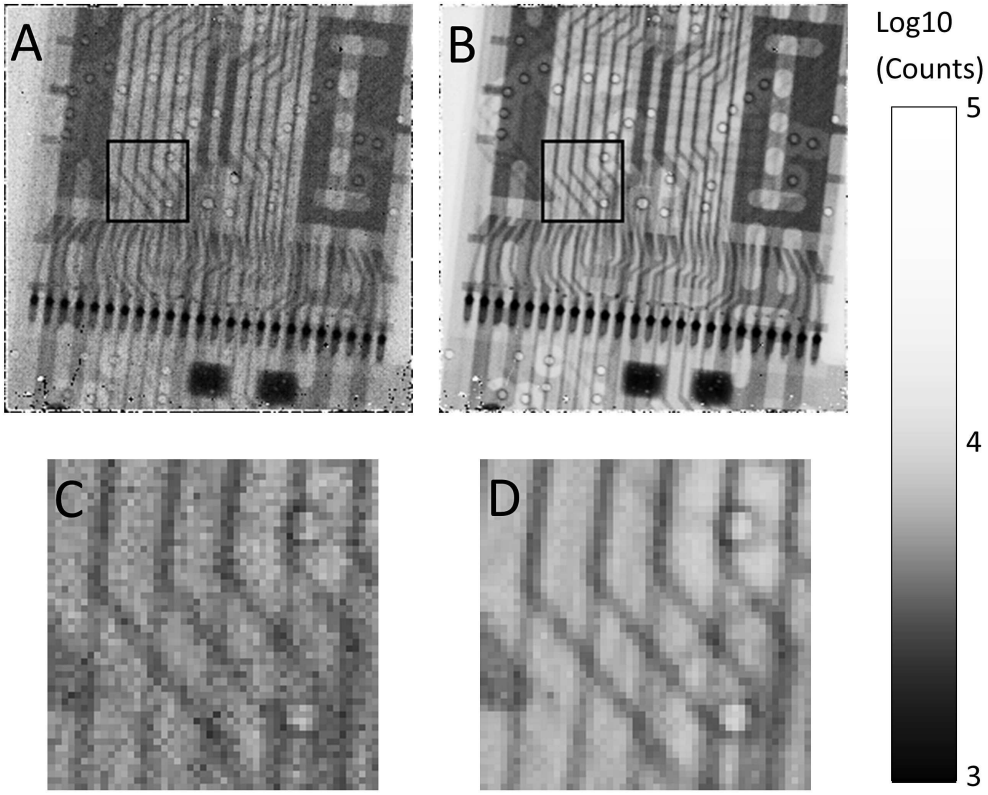

Figure 11. Images of part of a USB stick taken with the Ge detector at -100V bias, and -110°C and threshold setting 7.5 keV. Images are shown with a logarithmic scale, and consist of the sum of 300 acquisitions with 1s shutter time each. (A) Full-chip raw image with no flat field correction applied. (B) Full-chip flat-field corrected image. (C) A zoom into the raw image A. (D) A zoom into the flat-field corrected image B.

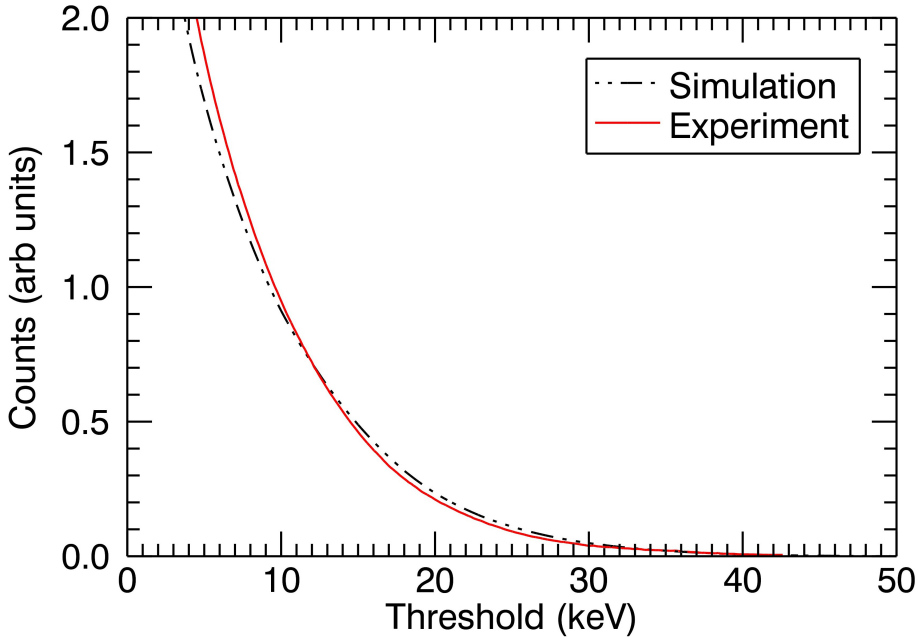

Figure 12. Experimental and simulated threshold scans for the Ge detector, using the Ag-target X-ray tube with 50kV tube voltage and -100V detector bias.

used to find the relationship between threshold settings on the readout chip and the effective energy threshold, which was approximately 50 electrons per threshold step. This corresponds to lower gain than the reported 37 electrons per threshold step for the Medipix3RX chip in Super-High Gain Mode [9]. However, this calibration is approximate, and during these measurements the threshold settings used on the chip were chosen for low power consumption and high leakage current tolerance, and the chip was operated far below its usual operating temperature. So, the gain response of the detector should be investigated further once a test setup is built that can be used with a monochromatic source.

5.3 Effect of temperature on performance

The detector was tested at a range of temperatures from -100°C to -60°C, by turning the cooling system off and allowing the temperature to rise during acquisition. A USB connector was placed between the X-ray tube and the sensor, and 5 second images were taken using the X-ray tube. A bias of -100V was used in each case. The images at -100°C, -80°C and -60°C are shown in figure 13.

As the temperature increases, a few major changes can be seen. Firstly, the region of insensitive pixels at the edge of the detector grows in size from 1 pixel at -100°C to 8 pixels (440 µm) at -60°C. In each case, many pixels at the border between the sensitive and insensitive region are noisy. Secondly, the number of noisy pixels in the central sensitive region increases from 25 at -100°C, through 87 at -80°C, then rapidly increasing to 2900 at -60°C. Both of these effects can be explained by an increase in leakage current. Although Medipix3 pixel design is able to compensate for a certain level of leakage current — 9 nA per pixel under the chip settings used here — increasing leakage current will alter the amplifier's behaviour. First, the zero level in the pixel will shift

2014 JINST 9 P12003

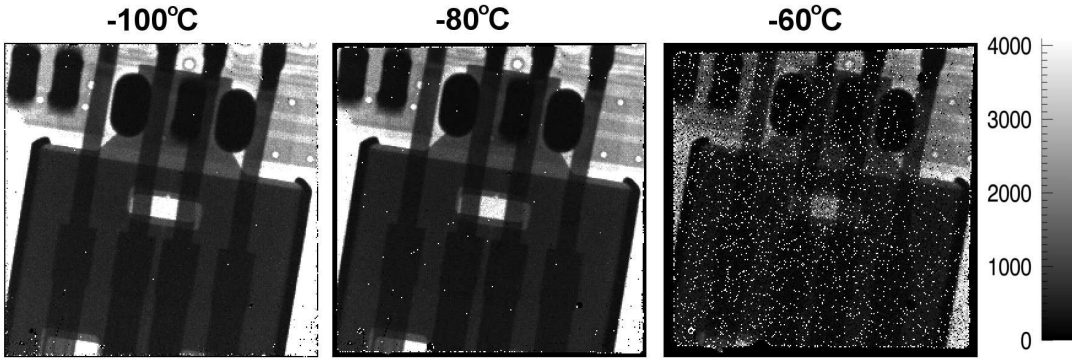

Figure 13. Images of a USB connector taken with the germanium detector at -100°C, -80°C and -60°C.

upwards as the integrating capacitor becomes filled, resulting in the pixel becoming noisy. This effect could be compensated to some extent by repeating the equalisation process. As the leakage current increases further, the amplifier will saturate, and the pixel will no longer count photons.

Additionally, in the image taken at -60°C, fewer counts can be seen in the illuminated regions. In germanium, the depletion voltage increases with temperature, with the test diodes showing at most 25V depletion voltage at -100°C and 130V -60°C. So, the reduction in counts at this warmer temperature can be explained by underdepletion.

6 Conclusions

A germanium sensor with 55 µm pixel size has been successfully hybridised with a Medipix3RX readout chip by indium bonding. The resulting sensor works, with a high proportion of the pixelated area working and a high unformity compared to most high-Z materials. The working temperature range of -80°C and lower agrees with the expected working range estimated from tests on germanium diodes. There is high edge leakage current in the sensor, which results in pixels near the edge becoming saturated with current. The high edge current was also seen in test diodes, so it is not a new problem with the hybridised sensor, but this will need to be improved to achieve a fully sensitive detector area.

Work has begun on further hybrid germanium sensors. The new sensors will also be bonded to Medipix3RX chips, but the wafers will include "hexa" sized sensors with 768 × 512 pixels that will be bonded to 6 readout chips. The guard ring region and edge processing will be adapted to reduce the edge leakage current. A more compact and transportable cooling chamber is also being designed, with a thin entrance window for X-rays and with most of the readout electronics outside of the vacuum to reduce the cooling power. This system will allow X-ray measurements with standard lab X-ray sources and at synchrotron beamlines.

References

[1] R. Ballabriga et al., *The Medipix3 prototype, a pixel readout chip working in single photon counting mode with improved spectrometric performance*, *IEEE Trans. Nucl. Sci.* **54** (2007) 1824.

[2] P. Kraft et al., *Performance of single-photon-counting PILATUS detector modules*, *J. Synchr. Rad.* **16** (2009) 368.

2014 JINST 9 P12003

[3] B. Henrich et al., *The Adaptive Gain Integrating Pixel Detector AGIPD, a detector for the European XFEL*, *Nucl. Instrum. Meth.* **A 633** (2011) S11.

[4] L. Jones et al., *HEXITEC ASIC: a pixellated readout chip for CZT detectors*, *Nucl. Instrum. Meth.* **A 604** (2009) 34.

[5] T. Poikela et al., *Architectural modeling of pixel readout chips Velopix and Timepix3*, 2012 *JINST* **7** C01093.

[6] E. Frojdh et al., *Mapping the X-ray response of a CdTe sensor with small pixels using an X-ray microbeam and a single photon processing readout chip*, *Proc. SPIE* **8142** (2011) 814208.

[7] L. Tlustos, G. Shelkov, and O.P. Tolbanov, *Characterisation of a GaAs(Cr) Medipix2 hybrid pixel detector*, *Nucl. Instrum. Meth.* **A 633** (2011) S103.

[8] D. Pennicard et al., *The LAMBDA photon-counting pixel detector*, *J. Phys. Conf. Ser.* **425** (2013) 062010.

[9] R. Ballabriga et al., *The Medipix3RX: a high resolution, zero dead-time pixel detector readout chip allowing spectroscopic imaging*, 2013 *JINST* **8** C02016.

[10] M. Bigas, E. Cabruja and M. Lozano, *Bonding techniques for Hybrid Active Pixel Sensors (HAPS)*, *Nucl. Instrum. Meth.* **A 574** (2007) 392.

[11] S.D. Gunapala et al., 1024×1024 *pixel mid-wavelength and long-wavelength infrared QWIP focal plane arrays for imaging applications*, *Semicond. Sci. Technol.* **20** (2005) 473.

[12] M.J. Wolf, G. Engelmann, L. Dietrich and H. Reichl, *Flip chip bumping technology - status and update*, *Nucl. Instrum. Meth.* **A 565** (2006) 290.

[13] D. Pennicard et al., *Development of LAMBDA: Large Area Medipix-Based Detector Array*, 2011 *JINST* **6** C11009.

[14] K.W. Ang et al., *Impact of field-enhanced band-traps-band tunneling on the dark current generation in germanium p-i-n photodetector*, *Appl. Phys. Lett.* **94** (2009) 223515.

[15] D. Pennicard and H. Graafsma, *Simulated performance of high-Z detectors with Medipix3 readout*, 2011 *JINST* **6** P06007.

2014 JINST 9 P12003